SWIRL DEVELOPMENT AND ENHANCED HEAT TRANSFER ANALYSIS OF FERROFLUID IN ELLIPTICAL DUCTS UNDER THERMAL-MAGNETIC-FLOW FIELDS COUPLING

by

Cuihua WANG [a], ***Wenquan ZHANG*** [a], ***Duo RONG*** [a], ***Zepeng JIA*** [a], ***Bin GONG*** [a*], ***and Jianhua WU*** [a,b]

[a] School of Mechanical and Power Engineering,
Shenyang University of Chemical Technology, Shenyan, China
[b] School of Chemical Engineering and Technology, Tianjin University, Tianji, China

Original scientific paper
https://doi.org/10.2298/TSCI230424198W

It is a new practical method to apply external magnetic field in magnetic working fluid to enhance heat transfer. In this paper, the swirl flow and heat transfer characteristics of ferrofluid in elliptical tubes under thermal-magnetic-flow fields coupling have been studied by using the finite volume method. The flow structure and secondary vortices evolution process of magnetic nanofluid in elliptical ducts under the action of the magnetic fields have been obtained. The effects of magnetic induction intensity and the ratio of major axis to minor axis of elliptical pipe on the flow and heat transfer performances have been main investigated. The results show that there is obvious secondary flow (with four vortices or eight vortices) on the cross-section and the swirling flow is gradually formed due to the coupling of thermal-magnetic-velocity fields. With the increase of the ratio of major axis to minor axis, the heat transfer enhancement effect with the application of external magnetic field is weakened. The comprehensive performance of flow and heat transfer are better at lower Reynolds number and higher magnetic induction intensity.

Key words: *heat transfer enhancement, ferrofluid, magenetic field, multi-fields coupling, elliptical duct*

Instructions

Magnetic nanofluids are a new class of heat transfer fluids with fluidity and magnetism, which can be prepared by dispersing superparamagnetic nanoparticles with diameters of 10-100 nm in the base fluid [1], due to the presence of van der Waals forces and electrostatic forces between nanoparticles, nanoparticle aggregation occurs. To enhance the stability of nanofluids, many researchers have conducted corresponding studies. Currently, nanoparticle aggregation in the fluid can be mitigated through methods such as altering the solution's pH, ultrasonic agitation, and the addition of dispersants [2]. Ferrofluid is one of the most common magnetic nanofluids. In ferrofluid, the diameter of particles can vary from 10-50 nm [3]. These particles are usually made of magnetite or ferrite [4]. In the absence of magnetic field, the magnetic nanoparticles are uniformly dispersed in the base fluid, and the particles do not show magnetism. The mechanism of enhancing heat transfer of the fluids is the same as that of ordinary nanofluids. In the presence of a magnetic field, magnetic particles in a nanofluids are instantly arranged in order according to the direction of the magnetic field and they are magnetized. After magnetization, the flow, heat transfer and particle movement of magnetic nanofluids can

* Corresponding author, e-mail: wch-7855@163.com

be controlled by an external magnetic field to achieve high heat transfer rate. Therefore, the use of magnetic nanofluids in the presence of external magnetic fields can be considered as an appropriate means to enhance forced convection heat transfer and fluid mixing, which are widely used in aerospace, nuclear industry, biomedicine and other fields.

Experiments are the most commonly method to explore the flow and heat transfer of magnetic nanofluids. It is found that the thermo-physical parameters, the type, intensity and direction of the magnetic fields, the section shapes of flow ducts, and the thermal boundary conditions all significantly affect the flow and heat transfer performances of the ferromagnetic fluids [5]. The experimental results of Lajvardi *et al.* [6] show that the addition of Fe_3O_4 nanoparticles in water does not increase the convective heat transfer coefficient, but under the action of magnetic field, the thermal physical properties of ferrofluids change and the convective heat transfer effect is significantly enhanced. Wahid *et al.* [7] found that the magnetic field strength has an optimal value in enhancing heat transfer. At this time, the magnetic susceptibility of nanoparticles reaches saturation, and increasing the magnetic field strength has little effect on enhancing heat transfer of ferromagnetic fluid. The results of Abadeh *et al.* [8] show that the heat transfer effect of ferromagnetic fluid in the circular tube under alternating magnetic field is better than that under constant magnetic field, and the effect is more significant at low frequencies. Mohammad *et al.* [9] pointed out that the alternating arrangement of magnetic fields can achieve better heat transfer than the alternating magnetic field. Sha *et al.* [10] found that the average convection heat transfer coefficient of magnetic nanofluids increased by 5.2% and 9.2%, respectively, under the action of vertical uniform magnetic field and gradient magnetic field, but decreased by 4.8% but when the uniform magnetic field parallel to the flow direction of the fluid was applied. In addition different magnetic field conditions, the experiments on different volume fractions and flow states of ferromagnetic fluids are also conducted [11]. Most experimental results show that the convection heat transfer coefficient of magnetic nanofluids is proportional to the volume fraction and magnetic field strength, and the effect of magnetic field on heat transfer enhancement is more significant at low Reynolds number.

In recent years, with the rapid development of CFD and numerical heat transfer, the use of CFD simulation methods to study the convective heat transfer performance of magnetic nanofluids under the control of external magnetic fields has attracted much attention. Ashouri *et al*. [12] simulated heat transfer behaviour of the magnetic nanofluids in tube side of countercurrent double tubes heat exchanger under magnetic field using two-phase Euler-Lagrange method. The results show that the maximum heat transfer efficiency under the simulated conditions is increased by 36.4% when the external magnetic field is applied. At the same time, the pressure drop also increases with the increase of magnetic field strength, nanoparticle size and volume fraction. Fadaei *et al.* [13] think that the magnetic field will cause the fluid to produce a volume force perpendicular to the flow direction and generate eddy currents, which increases the temperature gradient near the wall, and thus increase the Nusselt number. Bezaatpour and Rostamzadeh [14] reached the same conclusion when the influence of the uniform external magnetic field of Fe_3O_4-water nanofluids on the heat transfer enhancement of the finned tube compact heat exchanger were numerically studied. Also, it is figured out that employing an external magnetic field at low Reynolds numbers is much more appropriate. The numerical results of Pattanaik *et al.* [15] and Morteza *et al.* [16] confirm that the secondary flow plays an important role in enhancing the heat transfer of ferromagnetic fluids. The convective heat transfer is also related to the size, structure and other conditions of the tube. At present, there are disagreements on the influence mechanism of the magnetic nanofluids on convective heat transfer under the action of magnetic field [17].

Elliptical tube is one of the common special-shaped tubes in compact heat exchanger. When the working medium is water, the forced convection heat transfer coefficient of elliptical tube is higher than that of circular tube [18]. However, little is known about the convection heat transfer of ferrofluid in elliptical ducts at present. Based on this, CFD simulation is used to research the coupling characteristics of the thermal-magnetic-flow fields and heat transfer effects of ferromagnetic fluid in an elliptical duct in presence of the constant external magnetic field, and the effects of Reynolds number, magnetic field intensity, and the ratio of long axis to short axis of the section on the flow and heat transfer of ferromagnetic fluid are emphatically analyzed in this paper.

Numerical simulation

Physical model and boundary condition

The physical model of an elliptical duct used in the numerical simulations is shown in fig. 1(a). In the figure, a and b represent the major axis and minor axis of the ellipse, respectively, and the pipe length is $L = 120$ mm. No slip boundary condition is applied to the wall, and constant heat flux is used to heat the outer wall. The Fe_3O_4-water nanofluid with $\Phi = 3$ vol.% is used as the working medium and its inlet temperature T_{in} is 283 K and main flow direction extends forward along the Z-axis. The tube is considered to be at a uniform magnetic field in the Y-direction. Four models A_1-A_4 are set up in this paper, seen tab. 1 for the specific structural parameters. In order to compare the heat transfer effect later, the wall perimeter of each model is set equal to ensure the same heat transfer area.

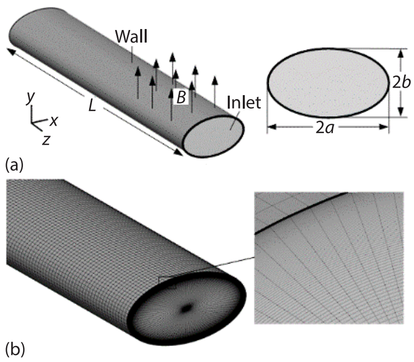

Figure 1. (a) Physical model and (b) grid distribution

Table 1. Structural parameters

Number	a [mm]	b [mm]	$2a:2b$	C [mm]	D [mm]
A_1	6.470	5.176	1.25	37.68	11.162
A_2	6.826	4.551	1.50	37.68	10.355
A_3	7.106	4.060	1.75	37.68	9.617
A_4	7.331	3.665	2.00	37.68	8.957

Note: $C = 2\pi b + 4(a - b)$ is the perimeter and is the equivalent diameter.

Governing equations

Assuming that the nanofluid is uniform without the viscous dissipation and chemical reaction, and the nanoparticle and the base liquid are in thermal equilibrium, the governing equation can be written:

$$\nabla(\rho) = 0 \tag{1}$$

$$\nabla(\rho VV) = -\nabla p + \nabla(\tau_{ij}) + F_m \tag{2}$$

$$\nabla(\rho V c_p T) = \nabla(k \nabla T) \tag{3}$$

where F_m and τ_{ij} are the magnetic force term and the shear stress tensor, respectively. τ_{ij} can be expressed in terms of the fluid viscosity and velocity gradient:

$$\tau_{ij} = \mu\left(\frac{\partial V_i}{\partial X_j} + \frac{\partial V_j}{\partial X_i}\right) - \frac{2}{3\mu\delta_{ij}\dfrac{\partial V_i}{\partial X_i}} \tag{4}$$

For the magnetic field is a uniform magnetic field in the Y-direction and F_m can be simplified:

$$F_m = \mu_0 x_m H^2 \frac{\left(-x_0\beta\right)}{1+\beta\left(T-T_0\right)^2}\frac{\partial T}{\partial y}\vec{J} \tag{5}$$

where μ_0 is the permeability of free space, x_m – the magnetic susceptibility, H – the magnetic field intensity, and β – the thermal expansion coefficient. For detailed derivation of the formula, please refer to [19].

Thermophysical properties

The correlation formulas of nanofluid density, specific heat, viscosity and thermal conductivity [20]:

$$\rho_\mathrm{nf} = \left(1-\Phi\right)\rho_\mathrm{f} + \Phi\rho_\mathrm{np} \tag{6}$$

$$\left(\rho c_p\right)_\mathrm{nf} = \left(1-\Phi\right)\left(\rho c_p\right)_\mathrm{f} + \Phi\left(\rho c_p\right)_\mathrm{np} \tag{7}$$

$$\mu_\mathrm{nf} = \frac{\mu_\mathrm{nf}}{\left(1-\Phi\right)^{2.5}} \tag{8}$$

$$k_\mathrm{nf} = k_\mathrm{f}\left[\frac{\left(k_\mathrm{np}+2k_\mathrm{f}\right)-2\Phi\left(k_\mathrm{f}-k_\mathrm{np}\right)}{\left(k_\mathrm{np}+2k_\mathrm{f}\right)+\Phi\left(k_\mathrm{f}-k_\mathrm{np}\right)}\right] + 5\cdot 10^4\,\vartheta\Phi\rho_\mathrm{f}c_{p,\mathrm{f}}\sqrt{\frac{k_0 T}{\rho_\mathrm{np}D_\mathrm{np}}}\,\mathrm{g}\left(\Phi,T\right) \tag{9}$$

where subscripts f, np, and nf are the basic fluid, nanoparticles, and nanofluids, respectively, ρ_np = 4950 kg/m^3, $c_{p,\mathrm{np}}$ = 640 J/kgK, k_np = 7 W/mK, and $k_0 = 1.3807 \cdot 10^{-23}$ J/K.

The ϑ in eq. (9) is a function related to the type and volume fraction of nanoparticles. Its function suitable for Fe_3O_4 derived by Goharkhah [21] through experimental research:

$$\vartheta = -0.673\Phi 3 + 0.2452\Phi 2 - 0.01782\Phi + 0.000487 \tag{10}$$

The expression of function g(Φ, T):

$$\mathrm{g}\left(\Phi,T\right) = \left(-6.04\Phi + 0.4705\right)T + 1722.3\Phi - 134.63 \tag{11}$$

The connection between the thermophysical parameters of the base fluid and the temperature is written [22]:

$$\rho_\mathrm{f} = 2446 - 20.674T + 0.11576T^2 - 3.12895\cdot 10^{-4}T^3 + 4.0505\cdot 10^{-7}T^4 - 2.0546\cdot 10^{-10}T^5 \tag{12}$$

$$\mu_\mathrm{f} = 2.414\cdot 10^{-5}\cdot 10^{\left[\frac{247.8}{T-140}\right]} \tag{13}$$

$$k_\mathrm{f} = -1.13 + 9.71\cdot 10^{-3}T - 1.31\cdot 10^{-5}T^2 \tag{14}$$

Performance parameters

The Reynolds number, the local heat transfer coefficient and the average heat transfer coefficient are defined:

$$\mathrm{Re}=\frac{\rho_{\mathrm{nf}}v_{\mathrm{nf}}D}{\mu_{\mathrm{nf}}},\ h_{\mathrm{local}}=\frac{q}{(T_{\mathrm{w,local}}-T_{\mathrm{nf}})},\ h_{\mathrm{ave}}=\frac{1}{A_{\mathrm{w}}}\int_{0}^{A_{\mathrm{w}}}h_{\mathrm{local}}\mathrm{d}S \tag{15}$$

The local Nusselt numbers along heated walls and the average Nusselt number of heated walls are obtained:

$$\mathrm{Nu}_{\mathrm{local}}==\frac{h_{\mathrm{local}}D}{k_{\mathrm{nf}}},\ \mathrm{Nu}_{\mathrm{ave}}=\frac{1}{Aw}\int_{0}^{Aw}\mathrm{Nu}_{\mathrm{local}}\mathrm{d}S \tag{16}$$

The friction factors and thermo-hydraulic performance are defined:

$$f=\frac{\dfrac{\partial p}{\partial Z}D}{2\rho_{\mathrm{nf}}v_{\mathrm{nf}}^{2}},\ THP=\frac{\dfrac{\mathrm{Nu}_{\mathrm{ave}}}{\mathrm{Nu}_{\mathrm{ave,0}}}}{\left(\dfrac{f}{f_0}\right)^{1/3}} \tag{17}$$

where v is the main velocity of fluid, A_{w} – the area of the heated wall, and $\partial p/\partial Z$ – the pressure drop gradient along the Z-direction. The subscript 0 refers to the value without magnetic field.

Numerical simulation and validation

The solution of the 3-D governing equations was made by the finite volume methods. For the discretization of the momentum equation and energy equation, second order upwind approach was employed. The standard SIMPLE algorithm was adopted for pressure-velocity decoupling and the convergence criterion was set as the relative residual less than 10^{-9}. A structured non-uniform grid shown in fig. 1(b) was used in the simulations and the gradual mesh refinement was performed near the wall with large velocity and temperature gradient. In order to achieve the mesh sensitivity analysis, average heat transfer coefficient, h, and friction factor, f, were calculated for different grid sizes for the model A_3 at Re = 1000 and B = 2000 G. The results are presented in fig. 2. It can be seen from the figure that when the number of grids increases to more than 2.2 million, the values of h_{ave} and f tend to be stable. When the mesh number is refined from 2.45 million 2.88 million, h_{ave} and f varied by only 0.05% and 0.001%. Thus, 2.45 million grids were selected for subsequent calculations in consideration of the accuracy of the results and the calculation time.

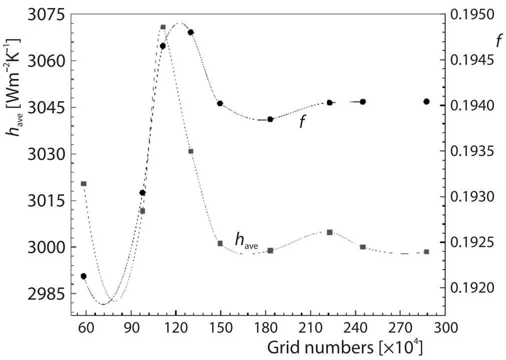

Figure 2. Grid independence test

Before the research, the reliability and accuracy of the results were verified and compared with the experimental results of the heat transfer of ferrofluid in the circular tube under an external magnetic field obtained by Sha *et al.* [10] and the simulation results of the laminar flow and heat transfer of ferrofluid in a double pipe mini heat exchanger under an external magnetic field obtained by Bezaatpour *et al.* [23]. The results in tab. 2 show that the simulated have in good agreement with the experimental results of Sha *et al.* [10] with the absolute maximum deviations of 3.98%, and the relative absolute difference of the simulated results of h_{ave} and f compared with the results of Bezaatpour are within 8.38% as well. The comparative results indicate that the simulation method is reliable and accurate.

Table 2. Verification of simulation results

B [G]	Flow	Reynolds number	h_{ave}			Δp		
			[10] [Wm^{-2}K^{-1}]	Simulation [Wm^{-2}K^{-1}]	Difference [%]	Literature [Pa]	Simulation [Pa]	Difference [%]
300	Cold flow	1600	1311.09	1314.85	0.29	–	–	–
		1720	1341.49	1316.97	–1.83	–	–	–
		1845	1372.53	1355.94	–1.21	–	–	–
		1960	1400.67	1363.40	–2.66	–	–	–
		2085	1431.83	1374.89	–3.98	–	–	–
B [G]	Flow	Reynolds number	[23] [Wm^{-2}K^{-1}]	Simulation [Wm^{-2}K^{-1}]	Difference [%]	[23] [Pa]	Simulation [Pa]	Difference [%]
		400	4122.51	3779.66	–8.32	1.45	1.35	–6.9
		800	4000.69	4174.26	4.34	2.89	2.95	2.08
		1200	3810.34	4011.65	5.28	4.49	4.81	7.13
		1600	3749.43	3944.42	5.2	5.86	6.06	3.41
		2000	3729.12	3937.36	5.58	7.52	8.02	6.65
	Cold flow	400	3736.84	3920.77	4.92	8.1	7.49	–7.53
		800	3604.76	3751.81	4.08	17.65	16.40	–7.08
		1200	3449.49	3651.71	5.86	26.82	26.34	–1.79
		1600	3388.8	3500.82	3.31	35.99	38.85	7.95
		2000	3358.46	3487.97	3.86	45.46	49.27	8.38

Results and discussion

In this paper, numerical simulations are carried out for different magnetic field intensities, B = 0-2000 G, Re = 1000-2000, and $2a:2b$, 1.25, 1.5, 1.75, and 2.0.

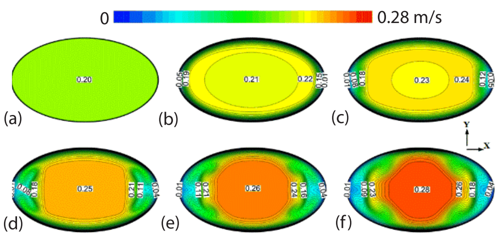

Figure 3. Axial velocity contours on different sections for the model A_3 at Re = 1500 and B = 2000 G; (a) Z = 0 mm, (b) Z = 10 mm, (c) Z = 20 mm, (d) Z = 40 mm, (e) Z = 60 mm, and (f) Z = 80 mm

Heat transfer mechanism of magnetic nanofluids under flow-magnetic coupling field

The axial velocity contours, the secondary flow vector and vorticity contours on different cross-sections which are 0 mm, 10 mm, 20 mm, 40 mm, 60 mm, and 80 mm away from the entrance for the model A_3 at Re = 1500 and B = 2000 G are displayed in figs. 3 and 4, respectively. Since secondary flow vector and absolute value of vorticity are symmetric about Y = 0 plane and X = 0 plane, they are only plotted for the 1/4 section of the elliptical tube.

It can be seen from fig. 3 that the axial velocity of the nanofluid is no longer uniform in the circumferential direction as the fluid-flows through the oval channel placed in an external magnetic field. Two symmetrical low speed zones appear in the region near the left wall and the right wall on the cross-section. As the fluid-flows forward, the two low axial velocity zones expand from the left and right sides toward the middle of the section gradually, therefore, the high speed zone in the centre becomes smaller and smaller, but the maximum axial velocity increases.

As shown in fig. 4, an obvious secondary flow is induced in cross-sections of the tube. When the cross-section is farther and farther away from the entrance, both the influence range and strength of the secondary vortex are gradually increase. Under the combined action of main flow and secondary flow, the ferrofluid-flows forward and swirling flow is generated in the duct.

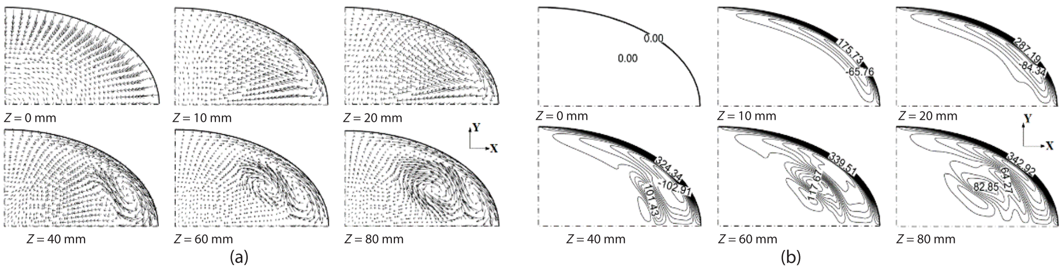

Figure 4. Secondary flow vector (a) and vorticity contours (b) on different sections for the model A_3 at Re = 1500 and B = 2000 G

In order to further explore the flow behaviour, the contours of Kelvin body force in Y-direction, F_m, on different sections for the model A_3 at Re = 1500 and B = 2000 G are obtained and shown in fig. 5(a). Considering the symmetry, in the following explanation of the temperature-flow-magnetic coupling field, 1/4 cross-section at the upper right will be described. As mentioned in eq. (5), the magnetic force is a function of the temperature gradient along the magnetic field direction. Seen from fig. 5(b), there is large temperature gradient near the heating surfaces, little temperature gradient in the centre zone. Therefore, the magnetic force is very intense near the heating surface, while the magnetic force is weak in the centre zone. The intense negative magnetic force near the upper heating surface drives the fluid to flow downward along the right inner wall, while the intense positive magnetic force near the lower heating surface drives the fluid to flow upward along the right inner wall. The two fluids meet at $Y = 0$ and turn to the left together due to the obstruction of the right wall. This secondary flow behaviour accelerates the mixing of nanofluid with lower axial-velocity on the right side of the section, disrupts the thermal boundary-layers and enhances the convective heat transfer, thus generating

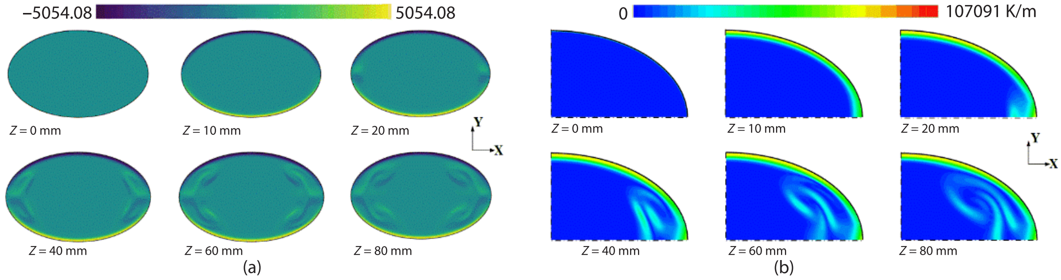

Figure 5. The contours of F_m (a) and temperature gradient (b) on different sections for the model A_3 at Re = 1500 and B = 2000 G

stronger positive magnetic force on the fluid in the region. Under the action of this magnetic force, the fluid continues to move to the upper left. In this way, a clockwise secondary vortex is formed on the upper right 1/4 cross-section, as shown in fig. 4. It is the magnetic force due to the temperature gradient that acts on the ferrofluid to form the swirling flow. As the fluid-flows forward, the stronger and stronger swirling flow accelerates the mixing of the fluid, intensifies the destruction of the boundary-layer, and affects the temperature distribution in turn. Therefore, the farther away from the entrance, the greater the temperature gradient of the fluid is in the low axial velocity zone on the right side of the cross-section, the greater the magnetic force is, and the intenser the swirl is. Consequently, the secondary flow on the 1/4 section far enough from the entrance is a double vortices structure. Therefore, the coupling relationship among the magnetic field, velocity field and temperature field of ferrofluid is intricate and synergistic.

Define dimensionless parameter $X' = [(a + X)]/2a$. For the model A_3 at Re = 1500 and B = 2000 G, the distribution of $\mathrm{Nu_{local}}$ on the heated surface of different sections along X' is shown in fig. 6. Consider symmetry about Y = 0 plane, it is only plotted for the upper half of the elliptic tube. As shown in fig. 6, the distribution of $\mathrm{Nu_{local}}$ along X' on the same heating surface is symmetric about X' = 0.5. When the ferrofluid is near the entrance, the values of each $\mathrm{Nu_{local}}$ on the heating surface are larger and the maximum value appears at the top of the heating surface. With the increase of Z, the $\mathrm{Nu_{local}}$ values on the heating surface show a decreasing trend, and another two $\mathrm{Nu_{local}}$ peaks appear. It can be seen from figs. 3-5 that the two peaks of $\mathrm{Nu_{local}}$ appeared on the heating surface are near the two centres of the secondary vortices, respectively, which indicates that the heat transfer of the ferrofluid is the best near the centres of the secondary vortices and the demonstrated swirling flow that accelerates ferrofluid mixing and thins the thermal boundary-layer is the main cause for improving convective heat transfer of ferrofluid. In the area close to X' = 0 and X' = 1, the velocity is very small which makes the heat transfer very poor. Therefore, the values of $\mathrm{Nu_{local}}$ at the left and right ends of the heating surface are very small.

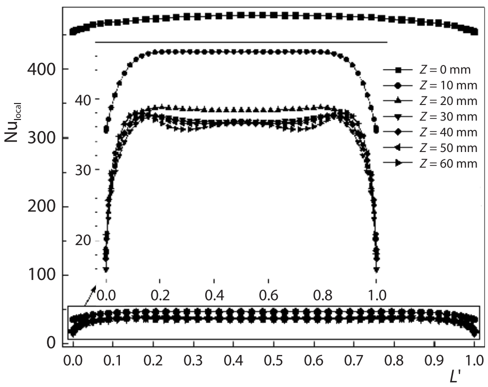

Figure 6. Variation of $\mathrm{Nu_{local}}$ on the heated surface of different sections for the model A_3 at Re = 1500 and B = 2000 G

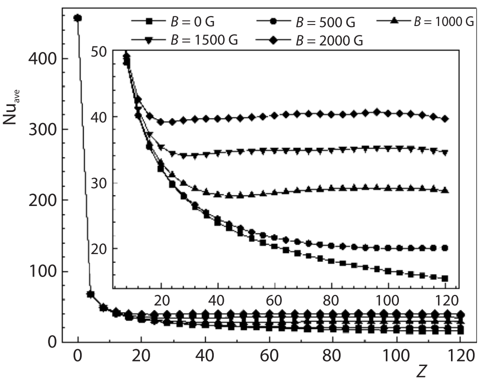

Figure 7. Variation of $\mathrm{Nu_{ave}}$ along Z under different magnetic field intensities for the model A_3 at Re = 1500

The evaluation of flow and heat transfer performance for different models with different magnetic field intensity

The variation of $\mathrm{Nu_{ave}}$ along Z under the influence of different magnetic field intensities for the model A_3 at Re = 1500 are illustrated in fig. 7. Since fluid mixing and thermal boundary-layer destruction are the main mechanisms for enhancing heat transfer, both of them are intensified with the increase of magnetic field strength. Therefore, as shown in fig. 7, the convective heat transfer increases with the increase of magnetic field intensity. The Nu_{ave} decreases at first, then slightly increases along the Z-axis. It is that the effects of magnetic field on ferrofluid-flow and heat transfer are weak near the entrance, but the thinner thermal boundary-layer still makes convective heat transfer better. As the fluid-flows forward, the thermal boundary-layer gradually thickens and Nu_{ave} decreases. Then, the effect of external magnetic field to enhance heat transfer began to manifest, and the stronger the magnetic field is, the closer the position where the magnetic field begins to play a visible role is to the entrance. When $Z > 50$mm, the Nu_{ave} under the external magnetic field are almost unchanged with a slight increase, which indicates that the synergistic relations among temperature-flow-magnetic fields is relatively stable here. The slight increase of Nu_{ave} may be attributed to the decrease of viscosity of ferromagnetic fluid with the increase of temperature along Z, which slightly strengthening the influence of swirling flow on the enhancement of heat transfer.

The relative axial velocity, v/v_{ave}, contours and the secondary flow vectors of full developed ferrofluid in four kinds of elliptical pipes with different ratios between long and short axes are shown in fig. 8, where v_{ave} is the average velocity of the cross-section. It can be seen from the figures that when the heating walls have the same area, the greater the ratio of long axis to short axis of the elliptical duct is, the greater the maximum central mainstream velocity. When Re = 1000 and the magnetic field intensity increases to $B = 2000$ G, the swirls in the four elliptical channels caused by the external magnetic field are intense enough that there are two vortices in opposite directions for the secondary flow on each 1/4 section. With the increase of the ratio of long axis to short axis, the two vortices gradually move to the right wall, and the mixing area driven by the swirl flow moves to the right wall as well, and the mixing range decreases. Due to the changes of flow field for different models, the beneficial effect of magnetic field on heat transfer also decreases with the increase of the ratio of long axis to short axis.

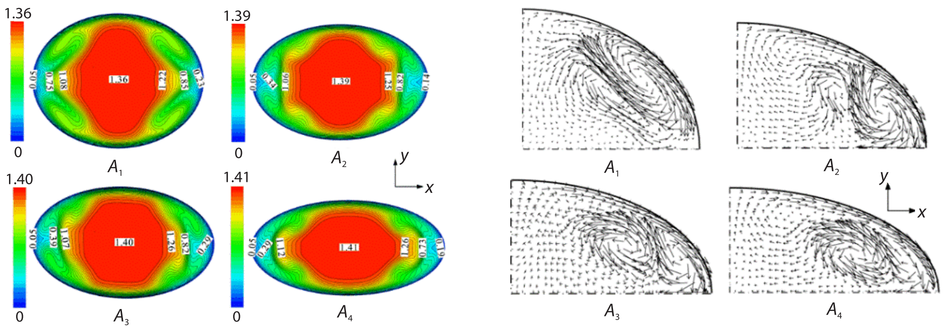

Figure 8. The relative axial velocity contour and secondary flow vector at the cross-section of Z = 100 mm for different models at Re = 1000 and B = 2000 G

The variations of Nu_{ave} and f of cross-section at Z = 100 mm with B for different models at Re = 1000 and Re = 1750 are shown in fig. 9. Under the same low magnetic field intensity, Nu_{ave} at large Reynold number is greater than that at small Reynold number in the same elliptical channel. However, when the magnetic field strength is large enough, there is the opposite result, that is, the Nu_{ave} is larger for smaller Reynold number and increasing Reynolds number will lead to a slight decrease in Nu_{ave}. It is obviously that the fluidic force due to the Reynolds number and the secondary flow caused by magnetic force affect the enhanced heat transfer of fluid together. For lower magnetic field intensity, since the secondary flow is weak, the influence of Reynolds number on the improvement of the average Nusselt number is dominant and the magnetic field plays a secondary role in enhancing heat transfer. However, for higher magnetic field intensity, heat transfer performance mainly depends on the magnetic field and increasing Reynolds number will shorten the action time of the magnetic field on the ferrofluid, thus making the decrease of Nu_{ave}.

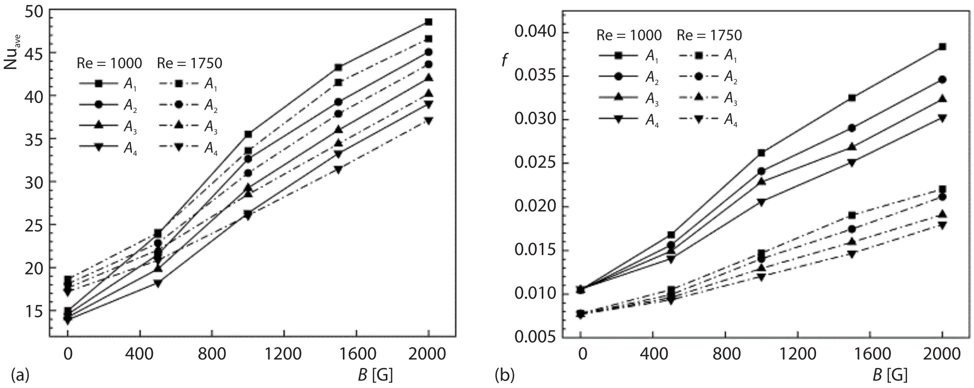

Figure 9. Variation of Nu_{ave} and f of cross-section at Z = 100 mm with B for different models

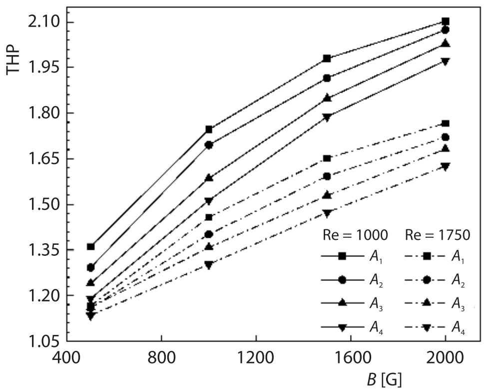

Figure 10. Variation of *THP* of cross-section at Z = 100mm with B for different models

It can also be observed in fig. 9 that both Nu_{ave} and f increase with B, which means that the magnetic field enhances heat transfer obviously, but also makes the fluid resistance increase significantly. Thermo-hydraulic performance given in fig. 10 considers both heat transfer and flow resistance for comprehensive evaluation of the enhancement method. It can be seen from fig. 10 that the *THP* of ferromagnetic fluid in an elliptical tube with an external vertical magnetic field is greater than 1.0. It implies that the method of using external magnetite field is beneficial since the heat transfer enhancement exceeds the increase of the flow resistance. The *THP* increases with the increase of B and decreases with the increase of Reynolds number, which gives the fact that it is more suitable to use external magnetic field for ferromagnetic fluid at low Reynolds number. When Re = 1000 and B = 2000, the Nu_{ave} of four models A_1-A_4 increases by more than 224.05%, 209.03%, 195.13%, and 180.15%, respectively compared with that without magnetic field, and the maximum *THP* is up than 2.10, 2.07, 2.03, and 1.97, respectively. The larger the ratio of the long axis to the short axis of the elliptical duct, the poorer the comprehensive thermal-hydraulic performance under the action of the magnetic field.

Conclusions

- Due to the coupling of temperature-magnetic-velocity fields, the ferromagnetic fluid in the elliptical duct gradually forms swirling flows, and there is a secondary flow with four vortices or eight vortices on the cross-section.
- Near the centres of the secondary vortices, there are Nulocal peaks on the heating surface. Along the Z-axis, the mean Nusselt number of the cross-section decreases at first, then

slightly increases, even if the synergistic relations among temperature-flow-magnetic fields is relatively stable.

- With the increase of the ratio of long axis to short axis, the heat transfer enhancement effect with the application of external magnetic fields is weakened
- The comprehensive performance of flow and heat transfer is better under the conditions of smaller ratio of long axis to short axis, lower Reynolds number and higher magnetic induction intensity.
- Within the scope of this study, application of the external magnetic field enhances the heat transfer of the models A_1-A_4 by more than 224.05%, 209.03%, 195.13%, and 180.15%, respectively, and the maximum of *THP* is up to than 2.10, 2.07, 2.03, and 1.97, respectively compared with those without magnetic field.

Acknowledgment

This study was financially supported by the General Program of the Educational Department of Liaoning Province (Grants No. LJKZ0447)

Nomenclature

A_1-A_4 – tube module area of wall surface, [m^2]
a, b – major axis and minor axis of the tube, [m]
B – magnetic flux density, [NA^{-1}m^{-1}]
C – perimeter of section specific heat, [kJkg^{-1}K^{-1}]
D – hydraulic diameter, [m]
F_m – Kelvin body force, [Nm^{-3}]
f – friction factor
H – magnetic field intensity, [Am^{-1}]
h – local heat transfer coefficient, [Wm^{2}K^{-1}]
k – thermal conductivity, [Wm^{-1}K^{-1}]
L – length of tube, [m]
Nu – Nusselt number
p – pressure, [Pa]
q – heat flux, [Wm^{-2}]
Re – Reynolds number
T – temperature, [K]
T_0 – 300 [K]
v – velocity in Z-direction, [ms^{-1}]
x_0 – differential magnetic susceptibility
x_m – magnetic susceptibility [$x_0/1 + \beta(T - T_0)$]
THP – comprehensive strengthening factor
X, Y, Z – directions

Greek symbols

δ – Kronecker delta
β – thermal expansion coefficient, [K^{-1}]
μ – dynamic viscosity, [Nsm^{-2}]
μ_0 – permeability of free space, [$4\pi\cdot10^{-7}$ NA^{-2}]
ρ – density, [kgm^{-3}]
τ_{ij} – shear stress tensor
Φ – volume fraction
ϑ – correction coefficient

Subscripts

f – fluid
nf – ferrfluid
np – nanopartical
w – wall
local – local
ave – average

References

[1] Salazar, J., *et al.*, Magnetic Iron Oxide Nanoparticles in 1040 nm Range: Composition in Terms of Magnetite/Maghemite Ratio and Effect on the Magnetic Properties, *Chemistry of Materials*, *23* (2011), 6, pp. 1379-1386
[2] Bahiraei, M., Hangi, M., Investigating the Efficacy of Magnetic Nanofluid as a Coolant in Double-Pipe Heat Exchanger in the Presence of Magnetic Field, *Energy Conversion and Management*, *76* (2013), Dec., pp. 1125-1133
[3] Malekan, M., *et al.*, Heat Transfer Modelling of a Parabolic trough Solar Collector with Working Fluid of Fe_3O_4 and Cuo/Therminol 66 Nanofluids under Magnetic Field, *Applied Thermal Engineering*, *163* (2019), 114435
[4] Sinatra, F. L., *Understanding the Interaction between Blood Flow and an Applied Magnetic Field*, University of South Florida, Tampa, Fla., USA, 2010
[5] Cherief, W., *et al.*, Effect of the Magnetic Field Direction on Forced Convection Heat Transfer Enhancements in Ferrofluids, *Eur. Phy. J. Applied Phy.*, *71* (2017), 1, 10901

[6] Lajvardi, M., *et al*., Experimental Investigation for Enhanced Ferrofluid Heat Transfer under Magnetic Field Effect, *Journal of Magnetism and Magnetic Materials*, *322* (2010), 21, pp. 3508-3513
[7] Wahid, C., *et al*., Parameters Affecting Forced Convection Enhancement in Ferrofluid Cooling Systems, *Applied Thermal Engineering*, *123* (2017), Aug., pp. 156-166
[8] Abadeh, A., *et al*., Experimental Characterization of Magnetic Field Effects on Heat Transfer Coefficient and Pressure Drop for a Ferrofluid-Flow in a Circular Tube, *Journal of Molecular Liquids*, *299* (2020) 112206
[9] Goharkhah, M., *et al*., Experimental Investigation on Convective Heat Transfer and Hydrodynamic Characteristics of Magnetite Nanofluid under the Influence of an Alternating Magnetic Field, *International Journal of Thermal Sciences*, *99* (2016), Jan., pp. 113-124
[10] Sha, L., *et al*., Experimental Investigation of Convective Heat Transfer Coefficient Using Fe_3O_4-Water Nanofluids under Different Magnetic Field in Laminar Flow, *CIESC Journal*, *69* (2018), 4, pp. 1349-1356
[11] Buschmann, M. H., Critical Review of Heat Transfer Experiments in Ferrohydrodynamic Pipe Flow Utilising Ferronanofluids, *International Journal of Thermal Sciences*, *157* (2020), 106426
[12] Ashouri, M., *et al*., Correlation for Nusselt Number in Pure Magnetic Convection Ferrofluid-Flow in a Square Cavity by a Numerical Investigation, *Journal of Magnetism and Magnetic Material*s, *322* (2010), 22, pp. 3607-3613
[13] Fadaei, F., *et al*., Heat Transfer Enhancement of Fe_3O_4 Ferrofluids in the Presence of Magnetic Field, *Journal of Magnetism and Magnetic Materials*, *429* (2017), May, pp. 314-323
[14] Bezaatpour, M., Rostamzadeh, H., Heat Transfer Enhancement of a Fin-and-Tube Compact Heat Exchanger by Employing Magnetite Ferrofluid-Flow and an External Magnetic Field, *Applied Thermal Engineering*, *164* (2020), 114462
[15] Pattanaik, M. S., *et al*., A Novel Magnetic Cooling Device for Long Distance Heat Transfer, *Applied Thermal Engineering*, *201* (2022), 117777
[16] Morteza, S., *et al*., Modelling and Simulation of Flow and Heat Transfer of Ferrofluid under Magnetic Field of Neodymium Block Magnet, *Applied Math. Mod*., *103* (2022), Mar., pp. 238-260
[17] Zang, X., *et al.*, A Review Oo Magnetic Field Effects on Flow and Heat Transfer in Magnetic Nanofluids, *Chemical Industry and Engineering Progress*, *38* (2019), 12, pp. 5410-5419
[18] Lei, S., *et al.*, Overall Thermal Performance Oriented Numerical Comparison between Elliptical and Circular Finned-Tube Condensers, *Int. J. of Thermal Sci.*, *89* (2015), Mar., pp. 234-244
[19] Ganguly, R., *et al.*, Heat Transfer Augmentation Using a Magnetic Fluid under The Influence of a Line Dipole, *Journal of Magnetism and Magnetic Materials*, *271* (2004), 1, pp. 63-73
[20] Xuan, Y., Roetzel, W., Conceptions for Heat Transfer Correlation of Nanofluids, *Heat Mass Trans*., *43* (2000), 19, pp. 3701-3707
[21] Goharkhah, M., *et al*., Experimental Investigation on Heat Transfer and Hydro-Dynamic Behavior of Magnetite Nanofluid-Flow in a Channel with Recognition of the Best Models for Transport Properties, *Exp. Therm. Fluid Sci*. *68* (2015), Nov., pp. 582-592
[22] Incropera, F., *et al*., Fundamentals of Heat and Mass Transfer, US Pat. 5, 328,671, 2011, 1048
[23] Bezaatpour, M., Goharkhah, M., Convective Heat Transfer Enhancement in a Double Pipe Mini Heat Exchanger by Magnetic Field Induced Swirling Flow, *Applied Thermal Engineering*, *167* (2020), 114801

Paper submitted: April 24, 2023
Paper revised: July 30, 2023
Paper accepted: September 7, 2023